High resolution 3D beam radiation pattern of harbour porpoise NBHF clicks with implications for passive acoustic monitoring

JDJ Macaulay[1*] (0000-0003-1309-4889), CE Malinka[2] (0000-0003-0138-8388), D Gillespie[1] (0000-0001-9628-157X), and PT Madsen[2,3] (0000-0002-5208-5259)

[1] *Sea Mammal Research Unit, Scottish Oceans Institute, School of Biology, University of St Andrews, East Sands, St Andrews, Fife, KY16 9LB, UK*

[2] *Zoophysiology, Dept. Bioscience, Aarhus University, 8000 Aarhus C, Denmark*

[3] *Aarhus Institute of Advanced Studies, Aarhus University, 8000 Aarhus C, Denmark*

* Corresponding author: jdjm@st-andrews.ac.uk

Abstract

The source properties and radiation patterns of animal vocalisations define, along with propagation and noise conditions, the active space in which they can be detected by conspecifics, predators, prey and by passive acoustic monitoring (PAM). Here we report the 4π (360° horizontal and vertical) beam profile of a free-swimming, trained harbour porpoise measured using a 27-element hydrophone array. The forward echolocation beam is highly directional, as predicted by a piston model, and is consistent with previous measurements. However, at off-axis angles greater than ±30°, the beam attenuates more rapidly than the piston model and no side lobes are present. A diffuse back beam is also present with levels about -30 dB relative to the source level. In PAM, up to 50% of detections can be from portions of the beam profile with distorted click spectra, although this drops substantially for higher detection thresholds. Simulations of the probability of acoustically detecting a harbour porpoise show that a traditional piston model can underestimate the probability of detection compared to the actual 3D radiation pattern documented here. This highlights the importance of empirical 4π measurements of beam profiles of toothed whales, both to improve understanding of their biology and to inform PAM.

Keywords

biosonar · piston model · narrow-band high frequency · passive acoustic monitoring

I. Introduction

Echolocating toothed whales ensonify their surroundings with short, powerful clicks and use weak returning echoes to navigate and find prey (Au, 1993). Broadly, these echolocation clicks can be split into four categories: sperm whales produce multi-pulsed 15-20 kHz transients (Møhl *et al.*, 2003), most dolphin and river dolphin species use short broadband clicks (Au, 1993; Ladegaard *et al.*, 2015), beaked whales produce slightly longer frequency-modulated pulses (Johnson *et al.*, 2004, 2006), whereas porpoises (Bassett *et al.*, 2009; Li *et al.*, 2007; Silber, 1991; Villadsgaard *et al.*, 2007) , *Kogia* (Madsen *et al.*, 2005), *Pontoporia* (Melcón, *et al.*, 2012), and six species of delphinids (Götz *et al.*, 2010; Kyhn *et al.*, 2009) have convergently evolved to produce narrow band high frequency (NBHF) clicks (~130 kHz). Despite this variation in the source properties of echolocation clicks, all toothed whales investigated thus far emit clicks in highly directional biosonar beams with similar directivity indices (Jensen *et al.*, 2018). Directing acoustic energy in this way generates higher source levels along the acoustic axis for the same power, which increases the range at which prey can be detected in a noise-limited environment whilst also limiting acoustic clutter (Madsen and Surlykke, 2013). A directional biosonar beam may also serve as a spatial filter of information (Madsen *et al.*, 2013), aid in the localisation of prey targets via a steep intensity gradient (Yovel *et al.*, 2010), and direct sound energy away from their acute auditory system that must detect and process weak echoes milliseconds after the emission of a powerful click (Schrøder *et al.*, 2017).

Toothed whales produce clicks by forcing pressurised air through their right pair of phonic lips in their nasal complex (Madsen *et al.*, 2013) which then is collimated using the skull and air sacs (Aroyan *et al.*, 1992) to form a directional sound beam that is radiated into the water via an impedance-matching fatty melon on the animal's rostrum (Cranford *et al.*, 1996; Cranford, 2000). The directionality of the click is seemingly defined by the size and conformation of phonic lips, skull anatomy, air sac configuration, melon structure and composition, as well as the frequency of the echolocation click. More generally, higher frequency sounds and larger physical structures will lead to a narrow beam, and lower frequencies and smaller radiating structure

to a less directional beam (Au and Scheifele, 1994). Thus, as smaller species are physiologically constrained by having smaller sound producing structures, they must use higher frequency signals to maintain the same narrow acoustic field of view as larger toothed whales (Jensen *et al.*, 2018). However, while a narrow acoustic field of view seems to have been a significant driver in the co-evolution of nasal structures and in the scaling of spectral composition of echolocation clicks across three orders of magnitude of size in toothed whales (Jensen *et al.*, 2018), other factors, such as acoustic crypsis to reduce predation, have likely also played a role. For example, high hearing thresholds of killer whales at frequencies above 100 kHz may have led to the convergent evolution of NBHF clicks across several small toothed whales (Kyhn *et al.*, 2013; Morisaka and Connor, 2007). For such NBHF species, the consequence of using NBHF clicks for both echolocation and communication is that their active space is small and directional ahead of the communicating animal (Clausen *et al.*, 2011; Sørensen *et al.*, 2018), or that they must employ lower frequency clicks for communication (Martin *et al.*, 2018). Thus, the source parameters and beam pattern of clicks used for both echolocation and communication are inextricably linked and valuable for understanding toothed whales sensory and evolutionary biology in the context of social behaviour, predator-prey interactions, foraging ecology and niche segregation (Madsen and Surlykke, 2013; Madsen and Wahlberg, 2007).

Quantifying toothed whale beam profiles usually involves the use of a compact array of hydrophones in a star or a linear and vertical configuration to record clicks from captive animals in controlled environments (e.g. Koblitz *et al.* 2012; Finneran *et al.* 2014; Smith *et al.* 2016) or from wild animals in close proximity (e.g. Rasmussen *et al.* 2002, 2004; Au & Herzing 2003; Zimmer *et al.*, 2005; Kyhn *et al.*, 2013; Jensen *et al.* 2015; Ladegaard *et al.*, 2015; Koblitz *et al.*, 2016). In most studies, only the narrow forward aspect of a beam (~$\pm$30°) is measured because the vast majority of the energy is contained in this small section of the beam profile, and it is that part that serves the animal in echolocation. Another attractive feature of using near on-axis apparent source levels (ASL, (Møhl *et al.*, 2000)) for beam estimation is that they can be conveniently fitted to a flat piston model to explain how most of the sound energy is radiated from the toothed whale forehead (Au, 1993). The piston model describes the beam attenuation with respect to angle relative to the acoustic

77 axis and depends entirely on only two parameters: the waveform of an on-axis echolocation click and the
78 functional aperture of the emitter (Au *et al.*, 1978; Strother and Mogus, 1970). When the on-axis waveform
79 is known for a given species, the equivalent aperture can be calculated by fitting the piston model to an
80 empirically measured beam (e.g. Beedholm and Møhl, 2006; Jensen *et al.*, 2015; Koblitz *et al.*, 2012). For
81 some applications, the equivalent aperture can be used to generate beam profiles of morphologically similar
82 species for which directly measured beam data have not been collected. However, while the piston model
83 works well for beam profile estimations ~±30° around the acoustic axis, it may not offer accurate measures
84 of ASL farther off-axis. In particular, the piston model will, by definition, mathematically not work beyond 90°
85 and yet click energy is radiated at those extreme off-axis angles (Finneran *et al.*, 2014).

86 While the consequences for biosonar operation may fully be explained within angles of ±30° off-axis and thus
87 successfully covered by the piston model, an understanding of the levels and waveforms of clicks farther off-
88 axis is relevant for studies of other aspects of toothed whale biology and management via passive acoustic
89 monitoring (PAM). In the correct circumstances, PAM can be used to calculate animal density - a key metric
90 for conservation regulatory frameworks. There are multiple analytic approaches to density estimation using
91 PAM which are usually dependent on the type of survey performed (Marques *et al.*, 2013). One possibility is
92 to simulate the probability of detecting animals using a Monte Carlo simulation based on pre-determined
93 auxiliary information on diving and acoustic behaviours. The efficacy of this approach is predicated on the
94 accuracy of the model inputs, one of which is the beam profile (Frasier *et al.*, 2016; Küsel *et al.*, 2011). Another
95 density estimation technique is the acoustic adaptation of spatially explicit capture/recapture (SECR) which
96 is based on animals ensonifying different numbers of receivers within a widely spaced hydrophone array
97 (Borchers *et al.*, 2015; Stevenson *et al.*, 2015); this is a relatively novel density estimation approach, but, if
98 used with toothed whale clicks or other directional vocalisations, would require a model of an animal's beam
99 profile (Stevenson, 2016). Knowledge of the beam profile is also a factor when designing hydrophone arrays
100 to localises and provide acoustic quantifications for different species (e.g. Zimmer *et al.*, 2008; Malinka *et al.*,
101 2020).

The potential importance of beam profiles, both in understanding the sensory ecology of animals and for informing PAM, has prompted several studies on the wider radiation of sound around toothed whales. The full or near-full horizontal beam profiles of clicks (±180°), burst pulses and/or whistles have been measured for common bottlenose dolphins (*Tursiops truncatus*) (Au *et al.*, 2012a; Branstetter *et al.*, 2012; Finneran *et al.*, 2014) and for a harbour porpoise (*Phocoena phocoena*) coarsely out to 130° (Hansen *et al.*, 2008). Whilst appropriate for their respective aims, these studies placed only a small number of hydrophones (5 to 8) around a stationary animal, leading to relatively poor spatial resolution (with the exception Finneran *et al.*, 2014, who used 35 hydrophones) and limited measurements to one horizontal and/or one vertical slice of the beam profile. The full 4π beam (all of the vertical and horizontal angles around a sphere) has been measured elegantly for a wild sperm whale using data from an acoustic tag deployed in tandem with a towed hydrophone array, although the nature of the equipment and sperm whale behaviour meant that on-axis beam measurements were clipped (Zimmer *et al.*, 2005).

Here we report on the full 4π beam profile of harbour porpoises. Harbour porpoises are a widespread but generally undemonstrative species with a vocal repertoire that consists entirely of stereotyped NBHF clicks. The forward beam profile of harbour porpoises has been measured multiple times on stationary, captive harbour porpoises. Au *et al.* (1999) recorded a 16° half power (-3 dB) beamwidth, which was confirmed using suction cup hydrophones attached directly to the harbour porpoise's melon (Au, 2006). Koblitz *et al.* (2012) measured a narrower symmetric -3 dB horizontal beamwidth of 13° and a vertically compressed beamwidth of 11°. Adaptive widening of the porpoise beam was suggested by Madsen *et al.* (2010), speculated upon by Wisniewska *et al.* (2012), and later demonstrated and quantified by Wisniewska *et al.* (2015), who showed a dramatic widening of the half-power beamwidth during buzzing (clicks with a high repetition rate used in the final phase of prey capture), in some trials increasing the -3 dB beamwidth from ~10° to 30°. The shy nature of harbour porpoises makes them difficult to study visually but they are a good candidate for PAM because, despite high attenuation in seawater (Ainslie and Mccolm, 1998), NBHF clicks are relatively unique in many regions, including North Atlantic shelf waters As PAM hardware becomes more cost-effective, acoustic

density estimation methods are likely to be more widely used to study harbour porpoises (e.g. Carlén *et al.*, 2018). Knowledge of the full 4π beam profile is an important aspect in both interpreting PAM data and potentially for density estimation calculations but has not been measured before. Here, we use a 27-channel hydrophone array to measure the full 4π beam pattern of a free-swimming captive harbour porpoise. The implications for the probability of detecting animals using PAM are explored by comparing the piston model measurements from previous literature with the empirically measured 4π beam pattern.

II. Materials and Methods

A. Recording system

Data were collected in February 2018 at Fjord & Bælt in Kerteminde, Denmark, where one harbour porpoise is housed in an outdoor sea pen (3 m deep x 8 m x 13 m; Fig. 1). 27 hydrophones were arranged around the periphery of the sea pen; these consisted of eight TC-4034 hydrophones (Teledyne RESON A/S, Slangerup, Denmark), 12 high-frequency, autonomous digital sound recorders (SoundTraps, Ocean Instruments, NZ) and seven TC-4013 hydrophones (Teledyne RESON A/S, Slangerup, Denmark), which were arranged in a star-array (as used in Ladegaard *et al.*, 2017) and placed near one corner of the sea pen (Figure 1).

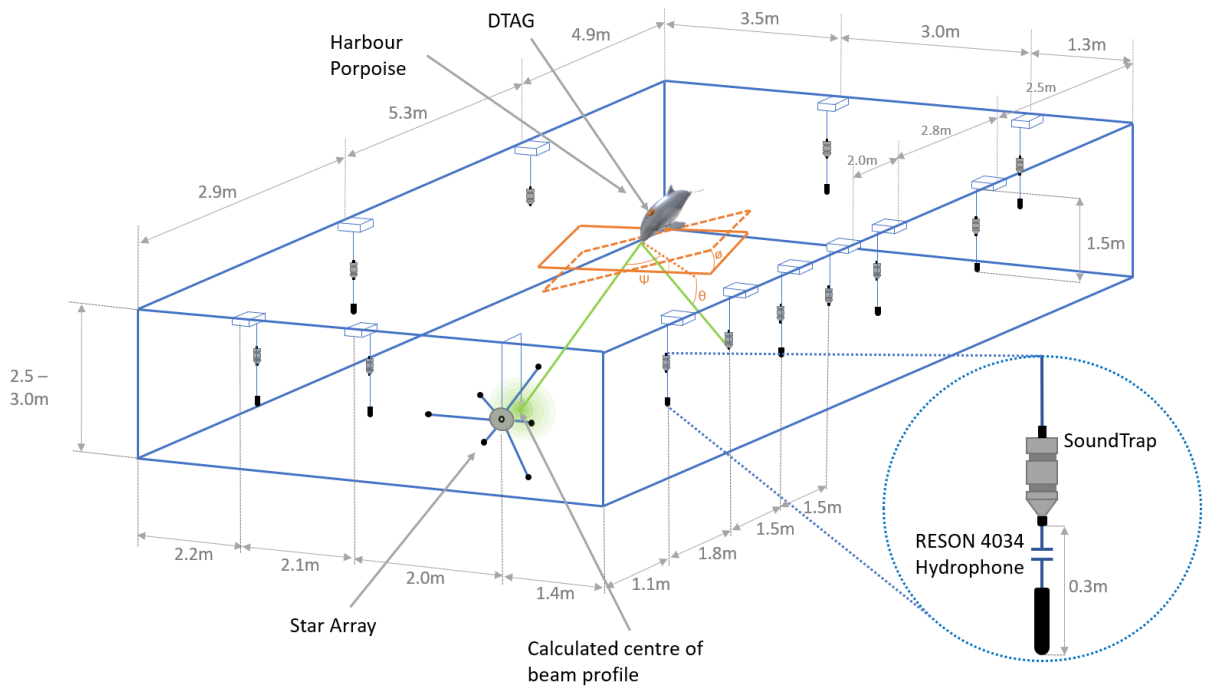

Figure 1. Diagram of the experimental setup (not to scale). The porpoise approached the 7-channel star-array. The received levels on the star-array were used to calculate the location of the centre of the porpoise beam. The (x,y,z) position of the porpoise was localised using the star-array. The centre of the beam and the localised porpoise position allowed for a vector to be calculated which was the acoustic axis of the animal. DTAG data then provided the roll angle of the porpoise. This created a full set of Euler angles (heading, pitch and roll). The received level was measured on every hydrophone (Reson and SoundTrap). A vector from each hydrophone to porpoise was calculated, and then projected onto the porpoise roll frame of reference, providing both the vertical and horizontal angle with the respect to the on-axis beam. The apparent source level for this horizontal and vertical angle was then calculated using the sonar equation, assuming spherical spreading. This process was repeated for every detected click to build up a picture of the beam profile.

SoundTraps were mounted above each TC-4034 hydrophone on steel poles (1 cm diameter) at depths of 1 m and 1.3 m respectively. These poles were mounted on floating pontoons. The central hydrophone in the star-array was at a depth of 1.2 m. The other six hydrophones in the star-array were located at even spaced angles (every 60°) around the centre hydrophone at alternating radial distances of 37.5 cm and 77.5 cm. The star-array was constructed from PVC and the solid poles holding hydrophones in place were 2cm diameter.

Outputs from hydrophones on the star-array were amplified by 60 dB using a custom-built amplifier box with low cut (1 kHz 1-pole high pass) and anti-aliasing (200 kHz 4-pole low pass) filters (both Butterworth) before digitization at 16-bit resolution using two synchronised 8-channel analogue to digital converters (NI 6356 USB data acquisition cards, National Instruments, USA), providing 15 synchronised channels with a 4 V peak-to-peak (*pp)* range and a 500 kHz sample rate. This resulted in clip levels of 164 and 157 dB re 1µPa for the TC-4034 and TC-4013 hydrophone recording chains respectively at 130 kHz. The sensitivity of the SoundTraps and TC-4013 hydrophones begins to drop off at ~150 kHz and the TC-4034 hydrophones reduce in sensitivity starting at ~200 kHz. Data from the NI cards were saved as 16 channel WAV files using PAMGuard (Gillespie *et al.*, 2008). The SoundTraps were programmed to record on high gain mode, clip level 174 dB re 1 µPa at 125 kHz. SoundTraps are autonomous single-channel units, and therefore time-synchronisation to channels on the array was completed after data collection.

The porpoise was equipped with a sound and movement tag (DTAG-4; (Johnson and Tyack, 2003)), mounted dorsally via suction cup behind the blowhole. Tag audio data were recorded at a sample rate of 576 kHz in 16-bit resolution (~170 dB re 1µPa clip level). The pitch and roll data recorded by the tag allowed for the full orientation of the porpoise to be calculated and thus enabled measurement of the full 4π beam whilst the porpoise was free swimming.

B. Experimental procedure

The captive porpoise used in all trials, Freja, weighed 62 kg and was approximately 22 years old. Freja was trained with positive food reinforcement to swim towards a familiar target and touch it, as she has done in several previous studies (e.g. Wisniewska *et al.* 2015; Ladegaard & Madsen 2019). The target, a 50 mm diameter aluminium sphere (TS -39 dB), was suspended on a monofilament line and placed in front of the centre of the star-array, at ranges of ~5-30 cm. One trial comprised a target approach over 10-14 meters that concluded with the porpoise putting the tip of her rostrum on the target, at which point the porpoise was bridged with a whistle and received a fish reward. The porpoise was not explicitly asked to produce

echolocation clicks while performing these tasks, but consistently did so as part of its normal behaviour. We saw a stereotypical reduction in source levels and inter-click intervals (ICI) during the approach, and a terminal buzz while moving up to the sphere to touch it, consistent with previous studies (Deruiter *et al.*, 2009; Ladegaard and Madsen, 2019) showing that she was echolocating to solve the task.

Target approaches were either completed with regular swimming or whilst rolling. Freja was given an audible and tactile signal to directly approach the target (n = 21), or was given a visual hand signal to actively roll while swimming in the direction of the target (n = 18) to provide for full 4π sampling of the acoustic radiation pattern. During rolling trials, one target approach comprised 1-3 rolls. 39 trials were run over four sessions over two consecutive days, with each session comprising up to 12 trials.

The porpoise sometimes wore opaque suction-cup eyecups during direct target-approach trials (on 7/21 target approach trials), so as to maximize the number of clicks produced, since porpoises have been observed to produce more clicks when blindfolded (Verfuß *et al.*, 2009). No eyecups were used during trials in which the porpoise was instructed to roll due to the visual cue used to request rolling.

The weather during the three days of data collection was fair, with no rain during data collection.

C. Calibrations

The 3D positions of each hydrophone were calculated to centimetre accuracy using a combination of measurements from a laser range finder (Bosch GLM 50 C Professional) and an accurate tape measure. Additionally, prior to each experimental session, each hydrophone was pinged for calibration with porpoise-like clicks (130 kHz, 10 cycles, generated by a waveform generator (model 33220A, Agilent Technologies, CA, USA)) from the same reference distance using a B&K 8105 hydrophone (Brüel & Kjær Sound & Vibration Measurement A/S, Nærum, Denmark) as a transducer.

The pinging trials were used to calculate the sensitivity of all hydrophones. A manual analyst marked out all clicks detected from the output hydrophone in PAMGuard (Gillespie *et al.*, 2008) which were then imported

into MATLAB (The Mathworks Inc., Natick, MA) and a 60 kHz 4-pole high-pass filter was applied. The relative peak-to-peak amplitudes of the received clicks on each hydrophone were measured and individual hydrophone sensitivities were calculated by comparing these levels to the levels on the central hydrophone on the star-array, assuming spherical spreading and a 0.04 dB/m transmission loss (at 130 kHz). This ensured that the relative sensitivities of each receiver were accurately calculated (standard deviation of ~1 dB in measurements), allowing for precise estimation of the beam profile whilst also permitting the absolute levels to be determined.

SoundTrap and DTAG clocks can drift at a rate of up to 20 parts per million, *i.e*. up to 72 ms per hour. The typical inter-click intervals of a harbour porpoise are <100 ms, and so clock drift on SoundTraps over several hours could potentially result in errors when matching clicks between different devices. Both DTAG and SoundTrap clocks were therefore aligned with the synchronised hydrophone array at the beginning of each session. Time alignment was performed in MATLAB by cross correlating the first 2 seconds of a detected click train. Each session was around 10 minutes, which equates to a maximum of 12 ms of clock drift and thus this provided sufficient time alignment for matching clicks, but did not allow for the SoundTraps to be used for acoustic localisation purposes.

D. Method Validation

To verify that we could estimate beam directionalities reliably, trials were also run with a known directional transducer, a TC-2130 transducer (Teledyne RESON A/S, Slangerup, Denmark), with a directivity index very similar to that of a porpoise (see Jensen *et al.* 2015). This transducer emitted a series of simulated NBHF clicks at 130 kHz generated by a waveform generator (model 33220A, Agilent Technologies, CA, USA). The TC-2130, mounted on a broomstick, was manually moved towards the star-array along the approximate swim path of the real porpoise while emitting clicks. The porpoise was not in the research pen while these trials were conducted. The data from this were analysed in the same manner as clicks from the real porpoise.

Additionally, the beam profile of the TC-2130 was accurately measured in a calibration tank. Details of the method validation can be found in the Supplementary Materials.

E. Data Analysis

Given the 3D approach tracks of a porpoise, detected porpoise clicks and properly time-aligned and calibrated hydrophones, it was possible to measure the beam profile of a free-swimming porpoise. Data analysis involved a five-stage process. First, 3D approach tracks were determined by detecting and localising received clicks on the star-array. Second, clicks received between the different hydrophones were matched. Third, received levels were measured. Fourth, the absolute orientation at each point on the track was calculated using the received levels on the star-array and roll measurements on the DTAG. Finally, the received levels and range to the porpoise at each hydrophone were used to calculate the apparent source levels with respect to horizontal and vertical angles of the porpoise's own reference frame. This process was performed for all detected clicks over multiple trials to build up a large number of measurements of the beam profile at different horizontal and vertical angles.

1. Click Detection and Localisation

In all trials, clicks received on each hydrophone were automatically extracted from raw sound files using PAMGuard (as in section II.C). Porpoise positions were then calculated using the known spatial hydrophone configuration and the time of arrival differences of the same click between the receivers. To minimise errors arising from echoes, only the star-array was used for localisation calculations. For every click detected on the central channel of the star-array, all possible combinations of porpoise clicks detected on other channels were determined. Time of arrival differences for each combination were calculated and a Simplex minimisation algorithm (Nelder and Mead, 1965) was used to calculate the range and direction to the porpoise. The time delay combination with the best fit to the localisation algorithm (*i.e.* the set of time delays which made most physical sense) was selected as the correct position of the porpoise. If this position was outside of the bounds of the pen it was discarded. A Savitzky-Golay FIR smoothing filter (Press and Teukolsky,

250 1990) (polynomial order: 3, window length: 9) was then applied to all localised positions within a specified
251 trial to construct a 3D interpolated track of the harbour porpoise approach, as shown in Figure 2.

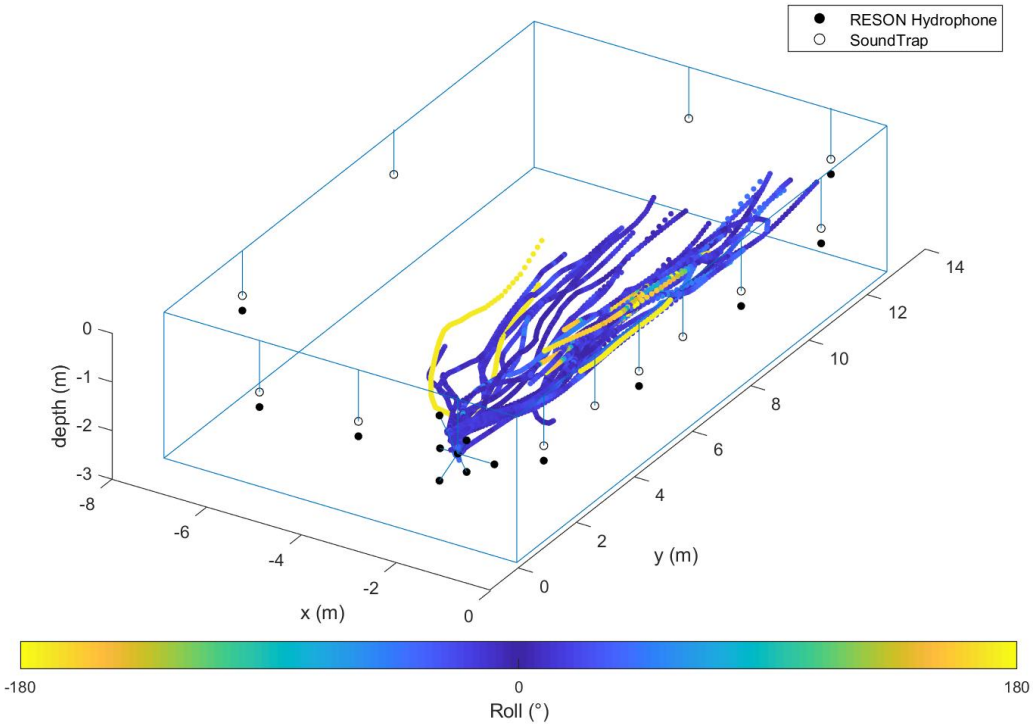

252

253 *Figure 2 Plot of localised swim paths of the harbour porpoise in 40 trials, to scale. The porpoise was tasked with swimming towards*
254 *a target just in front of the star-array. The colour of the track shows the roll of the porpoise. Most roll values are near 0° because a*
255 *single roll is a relatively brief event.*

256 ## 2. Matching Clicks

257 All detected clicks were imported into MATLAB. For every click received on the central channel of the star-
258 array, the same click was located on all other hydrophones around the sea pen. For each hydrophone, a time
259 window was calculated. The centre of the time window was based on the time for a click to travel from the
260 track position of the porpoise to the hydrophone, assuming a sound speed of 1500 ms^{-1}. For synchronised
261 hydrophones, the time window was ±1 ms from this time; for SoundTraps, which were not synchronised as

accurately, the time window was ±10 ms. If multiple clicks were detected within the time window, then the first click was selected, as any secondary click was likely an echo.

3. Received Level Calculation

For all matched clicks, the peak-to-peak received levels (RL) were calculated using the absolute sensitivity of each receiving hydrophone. RLs were measured by first filtering click waveforms with a 60 kHz 4-pole high-pass filter to reduce any ambient noise at lower frequencies.

4. Calculating Orientation

For each detected click, the acoustic axis vector of the porpoise was calculated using the star-array. An interpolated surface (2nd order polynomial in both *x* and *y*) was constructed based on the received levels of the click and positions of the hydrophones within the star-array using MATLAB curve fitting toolbox. The maximum peak of the surface was considered the received location of the central axis of the acoustic beam, and the height of the peak was the relative on-axis apparent source level from which all beam loss measurements were calculated. A vector from the on-axis beam location to the position of the harbour porpoise on the approach track was then calculated and roll from the DTAG was extracted. The roll, combined with the acoustic axis vector, created a full set of Euler angles for the porpoise (heading, pitch and roll).

5. Calculating the ASL ($\theta, \emptyset$)

A vector to the position of the porpoise on the approach track was then calculated for every hydrophone within the array, which detected the click. The vector was projected onto the rotational frame of reference of the porpoise using the Rodrigues rotation formula (Rodrigues, 1840). The horizontal angle of the projected vector with respect to the acoustic axis vector was the horizontal beam angle, θ. The vertical angle from the plane of the acoustic axis to the hydrophone was the vertical beam angle, $\emptyset$.

The beam apparent source level for this horizontal and vertical angle was calculated using the sonar equation (Eq. 1),

$$ASL_{pp}\,(\theta, \emptyset) = RL_{pp} + 20\log_{10} R + \propto R \qquad \text{Eq. 1}$$

where $ASL_{pp}\,(\theta, \emptyset)$ is the apparent source level (see (Møhl *et al.*, 2000)) with respect to horizontal (θ) and vertical angles ($\emptyset$). R is the range (in metres) from the hydrophone to the porpoise track at the time of the received click, RL_{pp} is the relative peak-to-peak received level, α is the absorption coefficient (0.04 dB/m for porpoise frequency; Ainslie & McColm 1998) and spreading loss is assumed to be spherical. The on-axis apparent source level was calculated in the same manner by considering RL_{pp} to be the maxima of the interpolated received level surface on the star-array. All ASL measurements were then normalised by subtracting the on-axis source level.

Every manually annotated click detected on the central star-array hydrophone over all trials was analysed in this way. Data were then filtered to attempt to remove spurious results; specifically, all clicks which were detected when the acoustic axis was calculated to occur outside of the 40 cm radius from the central hydrophone on the star-array were removed, as these often lead to inaccurate on-axis source level calculations. Measurements where the porpoise was within 0.5 m of a respective hydrophone were also removed as the log scale in Eq 1. means that small changes in the range at close ranges result in very large errors in ASL. Finally, the curve fitting algorithm occasionally registered a peak in the received level surface of the star-array when the true peak of the beam was in fact outside of the star-array. These spurious results could be removed by setting a lower amplitude limit of 156 dB re 1µPa *pp* to calculated on-axis source levels.

F. Piston Model

The beam profile was compared to a piston model. The piston model was generated by calculating the first order Bessel function that makes up the spatial transfer function of a circular surface with a diameter of 6.5 cm for horizontal angles and 8.3 cm for vertical angles (Koblitz *et al.*, 2012). The fast Fourier transform (FFT) of a porpoise click was multiplied by the complex conjugate of the Bessel function for a given angle and the peak-to-peak amplitude of the inverse Fourier transform of the result is the value of the piston model at that

angle (Beedholm & Møhl 2006). The position of side lobes on the piston model can be sensitive to the exact input waveform. To account for variation within on-axis clicks, a piston model was generated for every porpoise click detected on the central hydrophone array and within the filter parameters described in section II.E.5. The linear power outputs of the piston models for all these clicks were averaged and then converted to dB amplitude to give a final piston model.

G. Probability of Detection Simulations

Monte Carlo simulations can be used to calculate the probability of detecting animals on PAM instruments (Frasier *et al.*, 2016; Küsel *et al.*, 2011). There are multiple input parameters to such simulations one of which is the beam profile of animals. To test the implications of using an empirically measured beam profile, as opposed to a piston model, a Monte Carlo simulation for a harbour porpoise was developed which placed an animal at a random x,y location with a total range from a hydrophone between 0 and 750 m and maximum depth of 30 m. The simulated porpoises' source level, horizontal and vertical orientation, and depth at each location were parametrised from empirical measures of swim behaviour, source level and the beam pattern measurements. A received level was then calculated for a simulated hydrophone placed at the centre of the simulation x,y = (0,0) and thirty meters depth. A simulated click was considered detected if the RL_{pp} was above a specified minimum detection threshold; otherwise it was considered not detected. If detected, then the location was recorded as successful (coded 1), otherwise, the location was recorded as being unsuccessful (coded 0). 250,000 random locations were considered and a probability of detection then calculated by dividing the total number of successful detections by the total number of attempts. Each simulation was bootstrapped 20 times and averaged to increase precision.

Detection probability simulations were run for a range of detection thresholds (110 – 133 dB re 1µPa *pp*) and several different beam profiles. Three beam profiles were tested for these detection thresholds; the empirically measured beam, a full -90° to 90° piston model with the back beam set to -40 dB (the lowest value of the piston model), and the -30° to 30° piston model, with all other values set to -200 dB beam

attenuation (*i.e*. no side energy). The measured beam profile contained some holes at angles where no clicks were detected (see Figure 3) however the Monte Carlo simulation requires these to have some value to function properly. Therefore any holes at the edge of the beam profile surface (near ±180° horizontal and ±90° vertical) were assumed to be -45 dB (the lowest value of the measured beam profile) and any remaining holes were filled by interpolating the surrounding surface using Sibson interpolation (Park *et al.*, 2006).

Other parameters remained constant across all simulations. The porpoise was assumed to have a normal distribution of vertical orientation angles (mean = 0°, STD = 25°) a log normal depth distribution (shape = 2, scale = 3, max depth 30 m) and mean source level of 191 dB re 1µPa *pp* (Villadsgaard *et al.*, 2007) and standard deviation in source level of 5 dB.

The detection probability simulations assumed that clicks were always correctly classified, however it is a consequence of narrow beam profiles that off-axis angles clicks become highly distorted (Au *et al.*, 2012b). Automated PAM detectors may perform less efficiently in detecting these clicks and so the assumption that all clicks are equally as detectible if above threshold does not necessarily hold. A 'beam volume' for the measured beam profile was constructed to test the number of distorted clicks that might be detected by a PAM device. The beam volume is the 3D space inside which a recorder with a specified detection threshold would detect a porpoise click assuming a particular on-axis source level, spherical spreading loss, and accounting for absorption. The proportion of the total volume in which distorted clicks would be detected can then be estimated and used as a rough proxy for the percentage of distorted clicks a PAM device might detect.

III. Results

In total, there were 40 successful trials in which 100,264 clicks were detected over all hydrophones in the array. Of these, 15,154 were collected when the harbour porpoise was on-axis to the star-array, i.e. within a 40 cm radius of the central star-array hydrophone. During trials in which the porpoise was instructed to roll (no eyecups) only 699 clicks were detected, however, all trials contained some on-axis clicks.

The maximum variation in source levels of on-axis clicks used in beam profile measurements was 16 dB (minimum 156 dB re 1µPa *pp* and maximum 172 dB re 1µPa *pp*) with a mean of 161 dB re 1µPa *pp* and CI of ± 7 dB. This is slightly higher than other studies (e.g. Ladegaard and Madsen, 2019) however this is likely due to the exclusion of lower source level clicks from beam profile calculations as detailed in section II. E. 5

Beam profile measurements consisted of many overlapping measurements at different horizontal and vertical angles. An average beam profile surface was calculated by taking the median of all results within 2° (horizontal) by 2°(vertical) bins. Larger bins (5° x 5°) were used for horizontal angles > ±30° off the acoustic axis because there were fewer results at increasing off-axis angles (due to much lower signal to noise ratio). The median levels were plotted as a surface (Figure 3), demonstrating an intense forward beam and weaker diffuse energy behind the animal. Note that clicks were not detected for all possible angles, and as such are represented as blank spaces in the surface.

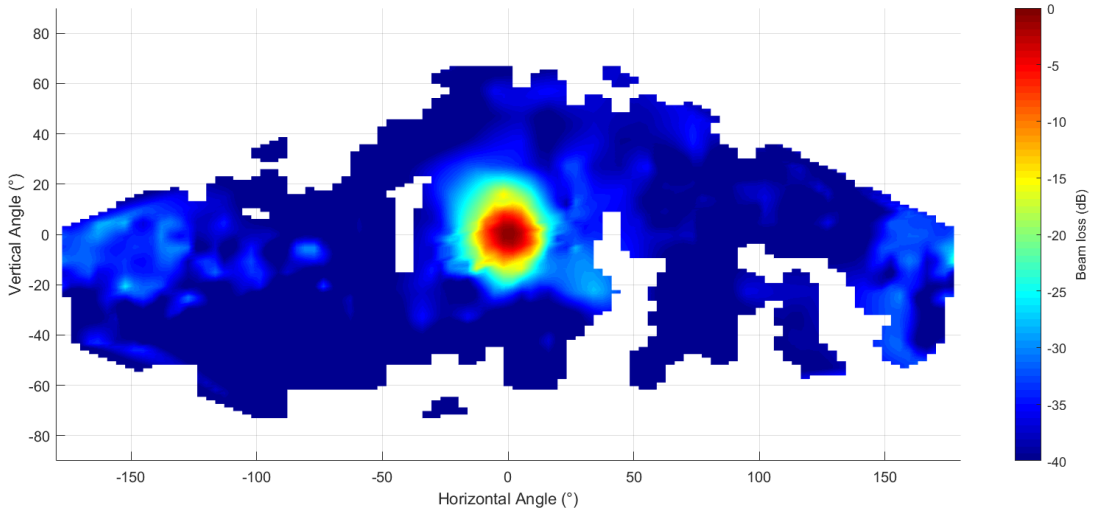

Figure 3. Porpoise beam profile showing full aspect coverage the beam. 2x2° grid bins used between ±30°, and 5x5° grids were used to take the median of the beam profile at all other angles. The intense forward beam is evident on-axis (0°, 0°). This attenuates rapidly towards ±90°. Behind the porpoise there is evidence of a diffuse acoustic energy which is ~25-30 dB less than the on-axis source level. Blank spaces indicate area where there were no measurements.

The spectra of clicks between ±3° vertical angle were plotted on a waterfall spectrogram with respect to absolute horizontal angle (i.e. ±θ are plotted as +θ). All clicks within the vertical angle bounds were grouped into 5° horizontal angle bins. The power spectra of all clicks were calculated and plotted on a surface in angle order for each 5° bin. The 5° bin surfaces were then stretched or compressed to a uniform width and plotted together to create a concatenated click angular spectrogram. Figures 4A and 4B show that the narrowband click spectrum breaks down at around 20° off the peak of the beam and is replaced by spectra with less predictable and more broadband components. It should be noted that the sensitivity of some of the hydrophones begins to drop off at around 150 kHz and that it is likely that many of the broader band components outside 100 to 150 kHz in Figure 4B are due to the much lower signal to noise ratio of clicks at larger off-axis angles. At off-axis angles (>20°) some of the angle bins also contain very few clicks, which likely causes some of the variation in standard deviation and mean measurements. However, in Figure 4B there is clearly structure to the peak frequency of sequential clicks in the 100 to 150 kHz band and thus stochastic noise introduced by lower signal to noise ratio (SNR) likely does not solely explain distortion of the click spectra.

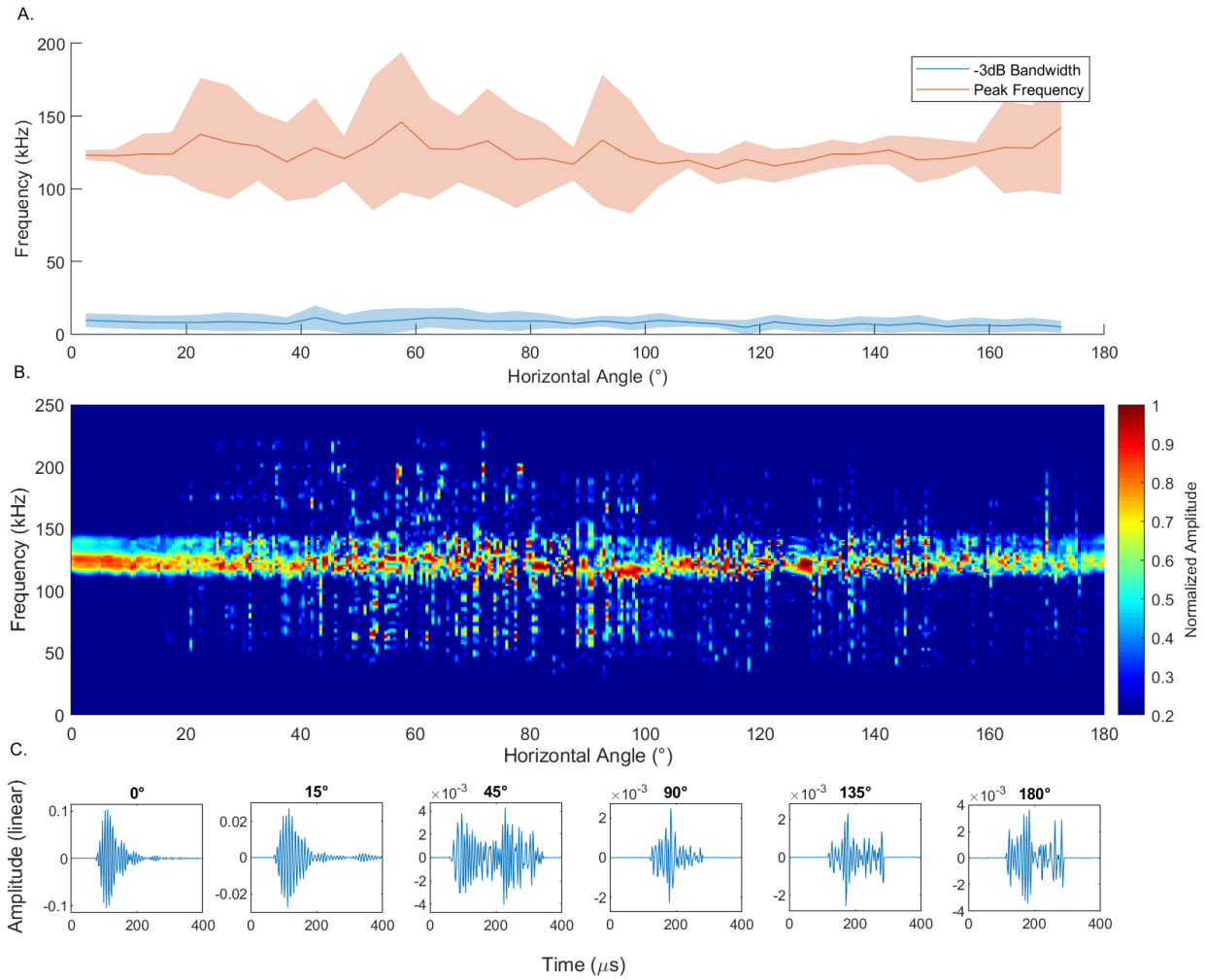

Figure 4. Frequency metrics, a waterfall spectrogram of clicks and examples of click waveforms with respect to horizontal axis. Clicks are split into 5° horizontal bins which contain all detected clicks within ±3° vertical angle sorted in order of horizontal angle. A. shows the mean peak frequency and -3 dB bandwidth, with standard deviation for each bin (Note that data points are plotted as the centre of each bin). and B. is a waterfall spectrogram of all clicks within each bin. The graphs show the break down in spectra beyond ~20° with peak frequency significantly more variable and with additional energy in higher and lower frequency components. It is likely that a portion of this distortion comes from the much lower signal to noise ratio of off-axis clicks, however, at off-axis angles and within the 100 to 150 kHz frequency band, there is clear structure to the spectra of sequential clicks that are not explianed simply by lower SNR. Note that the frequency axis limits on the waterfall spectrogram are between 50 and 200 kHz. C. shows and example of the waveforms of clicks extracted by PAMGuard at different angles. Note that some of these are zero padded to show a consistant time scale.

A. Comparison to the piston model

To assess how closely the piston model predicts off-axis beam attenuation, the empirically measured beam and a piston model were compared in two and three dimensions in Figure 5 and Figure 6. Figure 5 shows the raw beam for ±3° slices of the horizontal and vertical raw beam measurements plotted against a piston model with horizontal and vertical effective aperture diameters of 6.5 cm and 8.3 cm respectively (Koblitz *et al.*, 2012). The piston model was constructed of multiple received on-axis clicks and then averaged as described in section II.F. The standard deviation in directivity index was 0.15 dB and thus click waveform variation had little effect on the piston model other than suppressing side lobes.

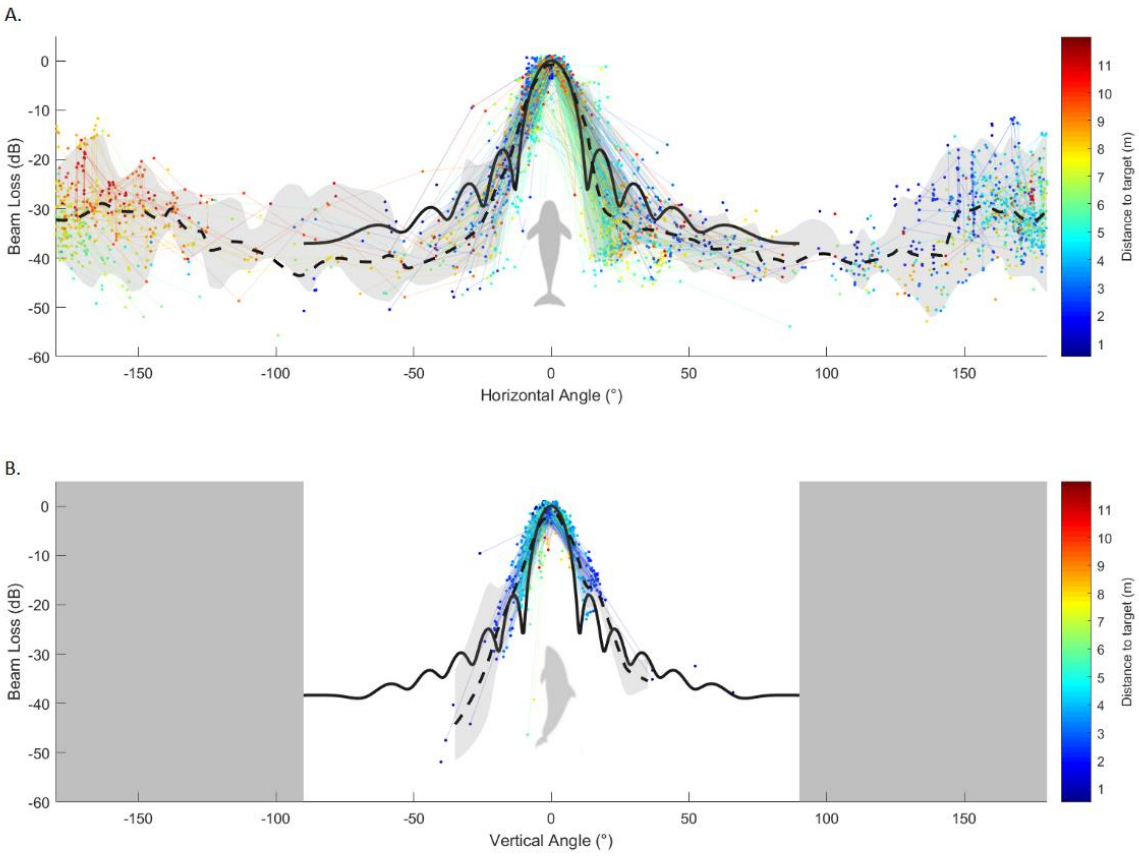

Figure 5. Raw beam data compared to the -90° to 90° piston model of an on-axis porpoise click for horizontal and vertical slices of the beam profile. A. shows all horizontal angles which have vertical angles between -3° to 3° and B. shows vertical angles

measurements which have horizontal angles between of -3° and 3°. Scatter points are back-calculated beam source levels with respect to angle. The solid black line is the average piston model results discussed in section II.F. The dashed black line shows the average beam measurement with grey area indicating the 95% confidence interval. The thin coloured lines group single clicks detected on multiple hydrophones together. Scatter points and lines are coloured by the distance to the target.

Figure 6 shows the measured beam and two piston models plotted as surface plots of expected received level assuming spherical spreading laws with an absorption coefficient of 0.04 dB m^{-1} (Ainslie and Mccolm, 1998) and an on-axis source level of 191 dB re 1µPa pp (an average recorded in a study of wild porpoises (Villadsgaard *et al.*, 2007)). For angles greater than 90°, the first piston model assumed beam attenuation was constant and equal to the lowest value predicted at ±90°, in this case -40 dB. The second piston model assumed beam attenuation was -200 dB (i.e. no energy) beyond ±30° (i.e. has energy only in the forward part of the beam). The plot shows the expected received level if a device were placed at (*x,y)* assuming a porpoise is facing in the *+y* direction at (0,0). This shows the typical acoustic space a wild animal might occupy in PAM studies.

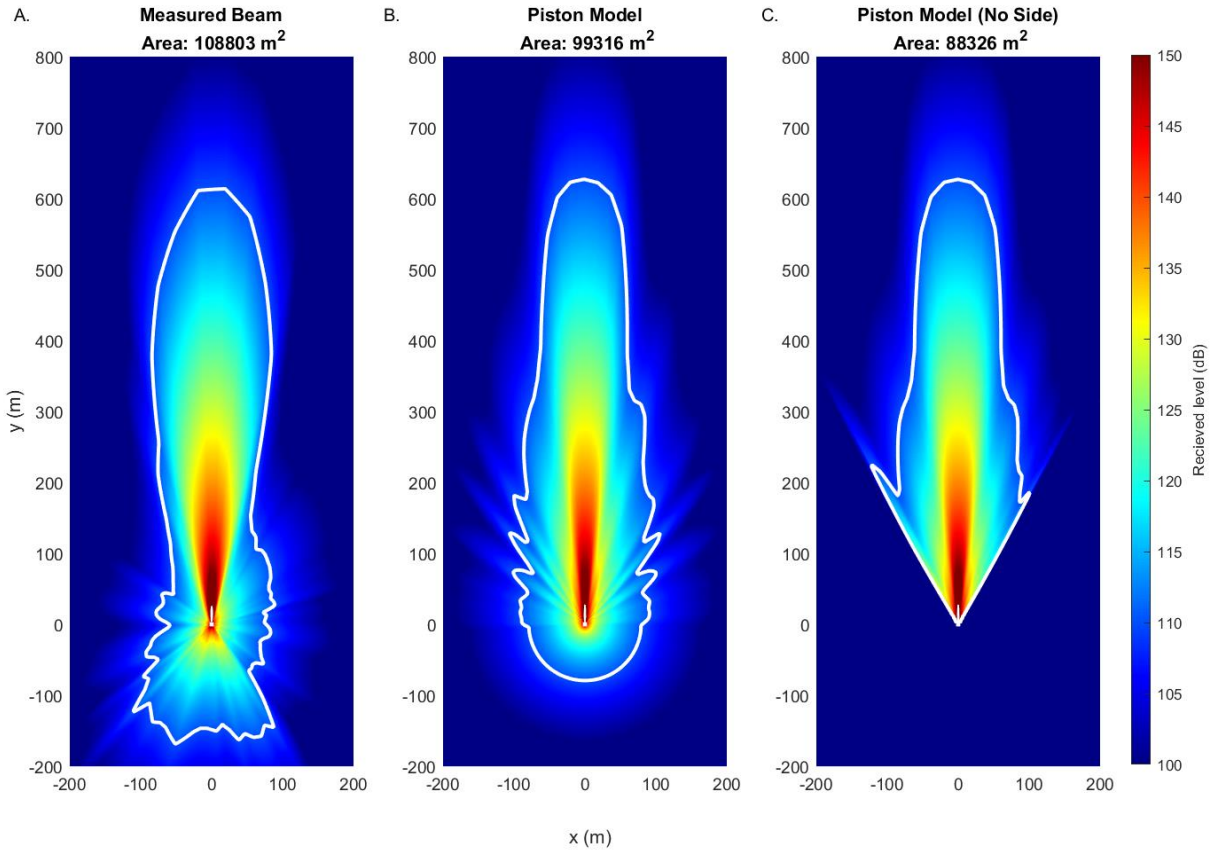

Figure 6. Beam profile detectability for an echolocation click with a SL of 191 dB re 1µPa pp. Each point on plot is coloured by the expected received level if a porpoise were facing in the y direction and located at (0,0). A. shows the measured beam profile for a harbour porpoise and B. shows piston model results, assuming a -40 dB uniform back beam (the lowest value of the piston model) using effective aperture diameter measurements. C. is the same piston as B. but with all energy removed past ±30° (i.e. only contains energy in the forward part of the beam). The lower colour limit of 100 dB re 1µPa pp was applied as this is below the usual limit (e.g. ~110 dB) for automated detection of clicks in PAM studies; thus darker blue areas in which a PAM device is less likely to detect a click The white line in both plots indicates what the detectable area would be for a PAM study using an automated detection algorithm with a peak-to-peak threshold of 110 dB re 1µPa pp. Titles show the area within the white lines.

B. Implications for PAM

There are clear differences between the measured and piston model beam in Figures 5 and 6. In the context of PAM it is important to understand whether the assumption of a piston model will make any appreciable difference to density estimation. Figure 7 shows the results of three Monte Carlo simulations of detection probability using the beam profiles in Figure 6. The probability here ($\widehat{P}$) is the probability of detection multiplied by a triangular step function and hence shows the probability of encountering a click, usually used

when analysing data from a stationary or drifting PAM devices. The area under the graph therefore directly divides the density estimation equation (Marques *et al.*, 2013). The results in Figure 7 show that, for a detection threshold of 110 dB (a typical value for an automated click detector) and source level of 191 dB re 1µPa *pp*, the full -90° to 90° piston model makes little different to $\widehat{P}$ and -30° to 30° piston model with no side energy underestimates $\widehat{P}$ by around half.

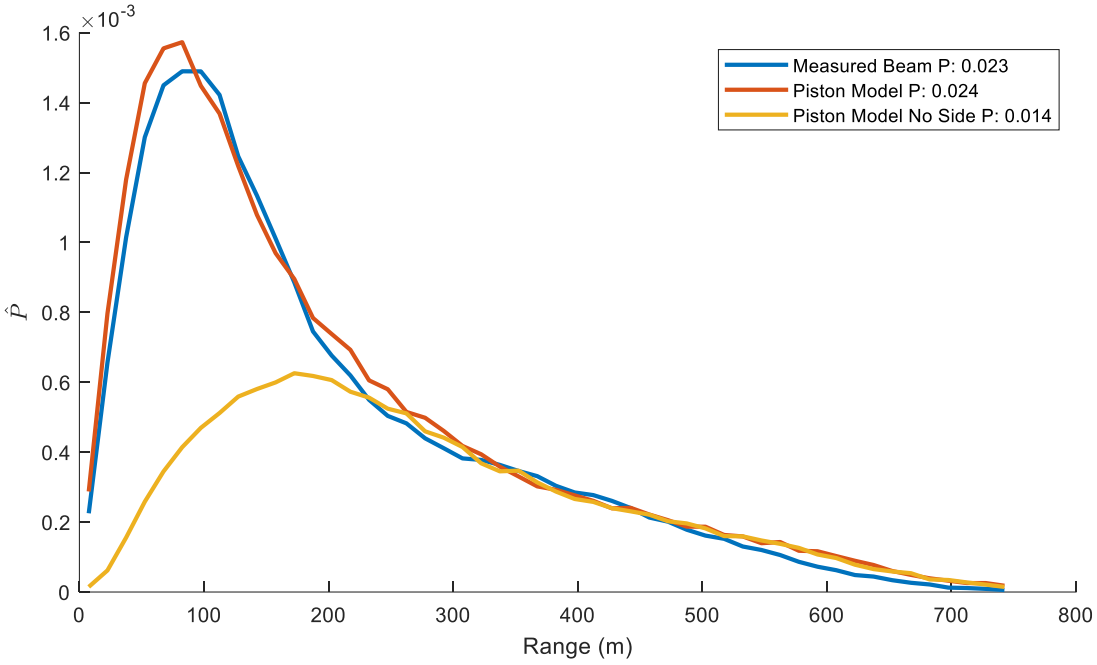

Figure 7. An example of the simulated probability of encounter ($\widehat{P}$) with respect to range for different beam profiles assuming a mean source level of 191 dB re 1µPa pp, a standard deviation of 5 dB and detection threshold of 110 dB re 1µPa pp. This is the probability that animal will be detected at a specified range assuming a homogenous distribution of animals around the sensor. The integral of these curves is a divisor of density estimation equation for fixed sensors.

Figure 8 shows how $\widehat{P}$ scales with different minimum detection threshold levels (i.e. the minimum click level required to register a detection on the PAM device) assuming a source level of 191 dB re 1µPa *pp*. The ratio of $\widehat{P}$ is not constant between beam profiles for different detection thresholds, with the piston

453 model with side energy underestimating $\widehat{P}$ by almost 30% at high detection thresholds, but only by around
454 5% at the lowest detection threshold source levels. The piston model with no side energy consistently
455 underestimates $\widehat{P}$.

456

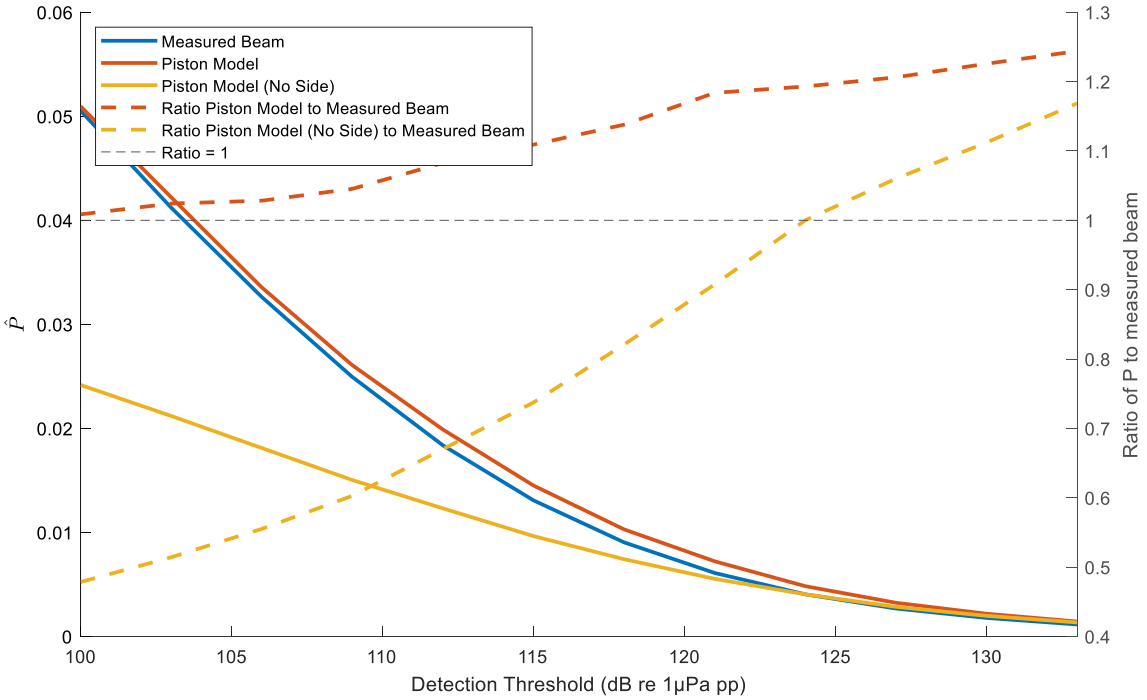

457

458 *Figure 8. Probability of encounter ($\widehat{P}$) modelled for different beam profiles as a function of detection threshold levels assuming a*
459 *source level of 191 dB re 1µPa pp. As expected, the probability of detection decreases with increasing detection thresholds for all*
460 *beam profiles (left axis). The dotted lines show the ratio of the probability of detection of the piston model beam compared to the*
461 *measured beam (right axis) and the grey horizontal line shows a ratio of 1.0, i.e. when detectability is equal to measured beam. This*
462 *shows that the ratio of the beam profiles does not remain constant and changes depending whether side energy is assumed. This*
463 *shows that the ratio of the probability of detection of the measured beam to each of the piston models does not remain constant.*
464 *For example, at lower detection thresholds the piston model with side energy has a probability of detection closer to the measured*
465 *beam profile. However, if no side energy is assumed, then the piston model is closer to the measured beam at higher detection*
466 *thresholds.*

In the above simulations it assumed that, as long as a click is above a certain amplitude threshold, it is detected. Figure 4 indicates a breakdown in the stereotypical spectra of NBHF clicks after around 20°. To test the potential consequence of this for PAM, beam volumes assuming a source level of 191 dB re 1µPa *pp* and detection thresholds between 100 and 130 dB re 1µPa *pp* were constructed and the percentage volume of > 20° section of the beam calculated. Figure 9 shows that, at high detection thresholds, the percentage of distorted clicks which would be detected by a PAM receiver is very low <5%, however at lower detection thresholds the number of distorted clicks is much larger, reaching ~50% for a threshold of 100 dB re 1µPa *pp*. Thus, depending on detection threshold (and/or source level), between 5% and 50% of click detections on PAM instruments would likely contain significant spectral distortion compared to on-axis clicks.

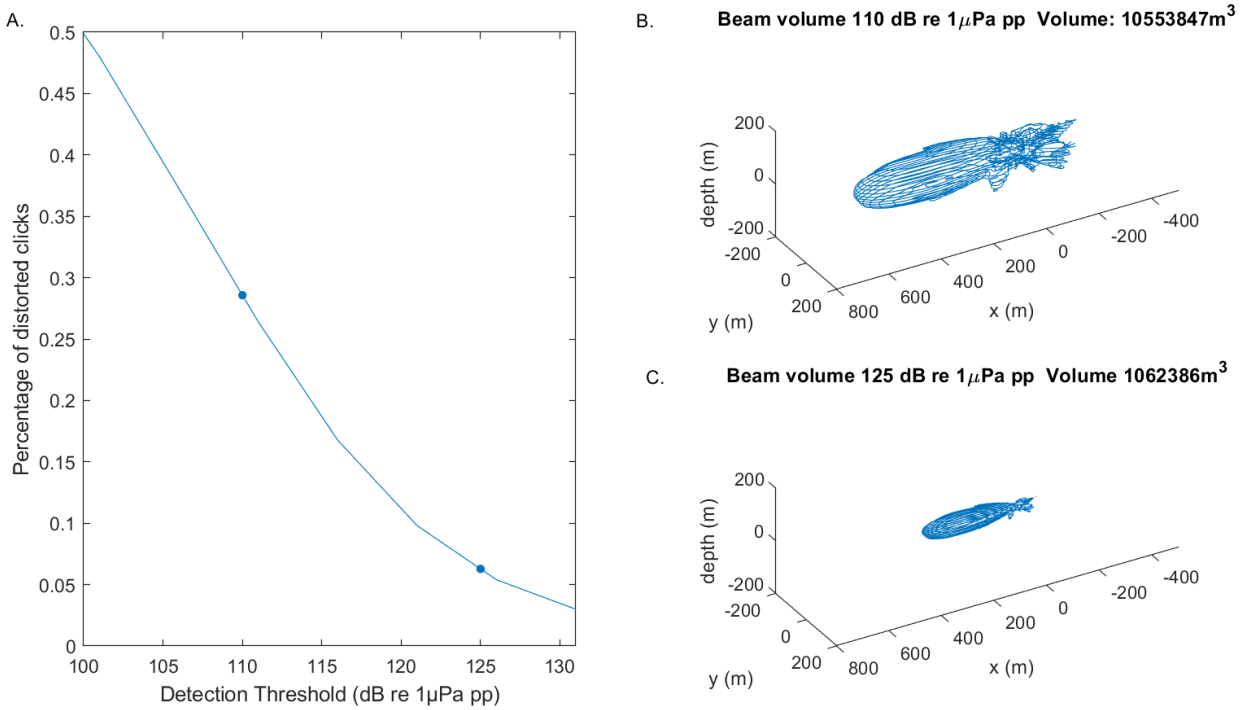

Figure 9. Plots showing the percentage of distorted clicks likely to be received by a PAM device and examples of beam volumes at differing detection thresholds. Plot A. shows the proportion of distorted clicks as a function of detection threshold, i.e. the number of clicks beyond ±20° off-axis. The two points indicate the detection thresholds of the example beam volumes shown in plots B. and C., (110 and 125 dB re 1µPa pp respectively).

IV. Discussion

In this study we confirm that the tightly focused forward beam with a DI around 24 dB (Figures 3, 5 and 6) of a harbour porpoise can be successfully modelled with a flat piston for angles between ±30° (Au, 2006; Koblitz *et al.*, 2012; Wisniewska *et al.*, 2015). However, at larger off-axis angles, the piston model underestimates the beam attenuation and creates a series of side lobes (Figure 5 and 6B) which were not evident in the measured beam profile. This side lobe suppression is likely formed through natural selection of harbour porpoise biosonars to i) increase SL for the same power, ii) reduce the amount of unwanted echoes in the form of clutter, iii) provide a spatial filter to aide localisation, discrimination and tracking of targets of interest, and iv) to direct sound of the outgoing click away from the ears to minimise forward masking of faint echoes returning milliseconds after click emission (Schrøder *et al.*, 2017). Thus, from an evolutionary perspective, it is perhaps not surprising that harbour porpoise biosonar has evolved both to minimise side lobes and to outperform a flat piston model in beam attenuation with angle. Side lobes are created from edge effects of the modelled piston aperture. However, there is no morphological structure which exactly mirrors the theoretical piston aperture in a porpoise. Thus, a more realistic equivalent aperture may be something which is not entirely radially symmetric and does not have a hard edge, minimising side lobes. We also tested the hypothesis that porpoises might use their melon to change the effective piston aperture, which, when averaged over many clicks, will reduce side lobes. However, averaging out a piston model using the horizontal 5.5 to 7.4 cm (mean 6.5 cm) apertures, as reported by Koblitz *et al.* (2012), still leaves two small side lobes at ±17°. Even if clicks are filtered to almost pure tones (between 125 and 130 kHz), which should increase the size of any side lobes, no side lobes are evident in the data (Supplementary Data 2). This suggests that the piston model, at anything other than on-axis angles, does not fully account for the morphological complexity of toothed whales. Madsen *et al.* (2010) noted that clicks produced by the phonic lips in the porpoise are initially quite broadband before they are filtered by waveguide coupling with the melon to form the NBHF click. This notion is supported here, where we see that the typical narrowband spectra of a NBHF click breaks down at about 20° (Figure 4), after which clicks are characterised by less predictable spectra.

When measuring the ASL farther off-axis, it appears that porpoises produce a diffuse back beam at 180° off-axis, some 30 dB down from the ASL. Madsen *et al.* (2010) have shown that harbour porpoises use their right pair phonic lips, which, in concert with air sacs and skull, collimate most of the produced sound energy through the melon to form a narrow forward beam. It is likely that some acoustic energy, especially when directed backwards, escapes this process, producing the back-end beam. Any baffled dipole source sound production system leads intrinsically to some diffuse waste acoustic energy as also observed for our Reson transducer calibrations (Supplementary Material). Thus, the diffuse and weak back-end beam of a harbour porpoise may simply be the remnants of a natural selection process towards a directional dipole source to work efficiently in a biosonar system for navigation or feeding. Whether it also serves a purpose of, for example, facilitating eavesdropping by calves to better trail their mothers during biosonar-based foraging dives may be plausible (Hansen *et al.*, 2008), but at this stage is entirely a speculative function for toothed whales at large. A similar weak back-end beam has also been reported in sperm whales (Zimmer *et al.*, 2005) with a very different bauplan of their hypertrophied sound producing nose.

Whilst the deviations between predictions from the piston model and the measured beam profile are interesting from physiological and biological perspectives, they also have consequences for PAM and density estimation. The distortion in click spectra at larger off-axis angles in Figure 4 will likely affect the performance of automated porpoise click classifiers, many of which are set up or trained for on-axis clicks (e.g. Cosentino *et al.*, 2019; Gillespie and Chappell, 2002). Such click classifiers may perform poorly with distorted off-axis clicks; which make up between ~5% and 50% of the detectible beam volume, depending on detection threshold as demonstrated in Figure 9. Thus, whereas signal to noise ratio is generally considered the primary driver of relative classifier performance, for harbour porpoises and most likely other toothed whales, the proportion of correctly *classified* clicks may also be dependent on the orientation of the animal and the detection threshold/on-axis source level.

The difference between modelled and empirically measured beam profiles can also significantly influence the probability of encountering clicks if side energy (>30°) is not taken into account. In Figure 7, the measured and full -90° to 90° piston beam model both have a higher probability of encountering a click at shorter ranges compared to the piston model without side energy. There are two interacting factors occurring here. First, the probability of *detecting* a click is increased slightly at shorter ranges because of the diffuse energy at the back of the measured and full piston beam profile Second, asthe range increases the number of animals within each range bin also increases and thus small increases in the probability of *detecting* a click result in disproportionally larger increase in *encountering* a click ($\hat{P}$). However, as range continues to increase, eventually any side and back beam energy becomes undetectable – at this stage the detectible energy is very similar for all beam profiles and thus at larger ranges $\hat{P}$ is almost identical. The point at which the back energy is no longer detected is therefore important in determining how different the overall value of $\hat{P}$ is. Thus at the high detection thresholds shown in Figure 8, any beam back energy will quickly fall below threshold and so the measured beam and piston model (no side) result in a similar $\hat{P}$. However, if the detection threshold decreases, the range at which back energy is detectible becomes larger and thus the piston model without side or back energy increasingly underestimates $\hat{P}$ compared to the measured beam profile and piston model with side energy. At very high detection thresholds, both piston models have a slightly higher $\hat{P}$ likely due to the side lobes, which are not present in the measured beam, continuing to make a small contribution to detectability.

The probability of encountering a click is a direct divisor of the density estimation equation for static PAM devices (Marques *et al.*, 2013) and so any differences in $\hat{P}$ propagate to estimates of animal density. Compared to the measured beam profile, the piston model with side energy over-estimated $\hat{P}$ by between ~5% to 25%, depending on the source level distribution of the animals in question. Assuming the piston model with no side energy and only a forward-facing beam resulted in an estimate of $\hat{P}$ which was between +20% and -50% compared to the measured beam profile. Thus, assuming a situation in which harbour porpoises are clicking at a source level of 191 dB re 1µPa *pp* and a typical detection threshold of 110 dB re 1µPa *pp*, the

555 piston model with no side energy would have almost doubled the density estimate but a piston model
556 assuming both side and back energy would be roughly correct. Although the exact error in the modelling of
557 the probability detection will be dependent on the survey type and combination of the many possible input
558 model parameters used in a Monte Carlo detection probability simulation, this indicates that beam profiles
559 are potentially a significant source of error in these models.

560 Empirical measures of the probability of detection are always preferred because they account for variation
561 in beam pattern, propagation, source level, *etc*. However, empirical measurements are often difficult to
562 obtain and simulation provides an alternative methodology to obtain measures of $\hat{P}$. Here we have shown
563 that, if using simulation methods for density estimation is indeed required, direct measurements of the full
564 4π radiation pattern is preferential wherever possible; if these are not available then an accurate piston
565 model assuming both side and back energy should be used. Alternatively, a forward piston model with a no
566 side energy but combined with a higher detection threshold may also be accurate.

567 V. Conclusion

568 Harbour porpoise produce an intense forward beam and much lower level diffuse acoustic energy to their
569 rear. The beam profile of a porpoise, relevant for assessing echolocation performance, can be modelled
570 successfully with a piston model at ±30° around the beam axis, but at off-axis angles of more than ±30°, the
571 measured beam shows greater attenuation than the piston model predicts, and no distinct side lobes can be
572 observed. Thus, porpoises have a slightly narrower acoustic field of view than predicted by the piston model.
573 We also document a weak and diffuse back beam with ASLs some 30 dB below the SL. We show with
574 modelling that there can be a substantially higher probability of detection when using the empirically
575 measured beam profile with a weak back-end beam, as opposed to the standard piston model, but this is
576 dependent on detection threshold and whether side and back energy in the piston model is assumed. As
577 such, this study highlights the need for synergy between sensory physiology, functional morphology and the

continued development of PAM methodologies and their subsequent interpretations, especially in the application of density estimation.

Acknowledgements

Thanks to the animal trainers J. Kristensen and F. Johansson for helping run the trials at Fjord & Bælt. Thanks to M. Wahlberg and J. Tougaard for lending hydrophones and SoundTraps, and to M. Johnson for access to a DTAG-4. Thanks to K. Beedholm, M. Wahlberg,J. Tougaard, M. Ladegaard, V. Janik, P. White and S. Northridge for helpful discussions and comments. Equipment and training time were funded by a Danish Research Council FNU grant to PTM. Thanks to our reviewers who were both very helpful and made this a better manuscript.

Software Availability

CetSim (https://github.com/macster110/cetacean_sim)

PAMGuard (www.pamguard.org)

PAMGuard to MATLAB library (https://sourceforge.net/projects/pamguard/files/Matlab/)

Ethics

The animals are maintained by Fjord&Bælt, Kerteminde, Denmark, under permit nos SN 343/FY-0014 and 1996-3446-0021 from the Danish Forest and Nature Agency, Danish Ministry of Environment.

Author Contributions

All authors conceived the idea; JDJM, CEM and PTM designed methodology; JDJM and CEM collected the data; JDJM and CEM analysed the data; JDJM lead the writing of the manuscript; DG advised on density estimation and PAM aspects. All authors contributed critically to the drafts and gave final approval for publication.

Supplementary Materials

See supplementary material at ***[URL will be inserted by AIP]*** for a description of the validation experiment of the beam measurement methodology.

See supplementary material at ***[URL will be inserted by AIP]*** for a brief analysis of the beam profile applying a narrow filter to all measurement in order to search for side lobes.

References

Ainslie, M.A., Mccolm, J.G., 1998. A simplified formula for viscous and chemical absorption in sea water. J. Acoust. Soc. Am. 103, 1671.

Aroyan, J.L., Cranford, T.W., Kent, J., Norris, K.S., 1992. Computer modeling of acoustic beam formation in Delphinusdelphis. J. Acoust. Soc. Am. 92, 2539–2545.

Au, W.W., Scheifele, P.M., 1994. The Sonar of Dolphins. J. Acoust. Soc. Am. 95, 585–586.

Au, W.W.L., 1993. The Sonar of Dolphins, Acoustics Australia. Springer New York, New York, NY.

Au, W.W.L., 2006. Acoustic radiation from the head of echolocating harbor porpoises (Phocoena phocoena). J. Exp. Biol. 209, 2726–2733.

Au, W.W.L., Branstetter, B., Moore, P.W., Finneran, J.J., 2012a. The biosonar field around an Atlantic bottlenose dolphin (Tursiops truncatus). J. Acoust. Soc. Am. 131, 569–576.

Au, W.W.L., Branstetter, B., Moore, P.W., Finneran, J.J., 2012b. Dolphin biosonar signals measured at extreme off-axis angles: Insights to sound propagation in the head. J. Acoust. Soc. Am. 132, 1199–1206.

Au, W.W.L., Floyd, R.W., Haun, J.E., 1978. Propagation of Atlantic bottlenose dolphin echolocation signals. J. Acoust. Soc. Am. 64, 411–422.

620 Au, W.W.L., Kastelein, R.A., Rippe, T., Schooneman, N.M., 1999. Transmission beam pattern and
621 echolocation signals of a harbor porpoise (Phocoena phocoena). J. Acoust. Soc. Am. 106, 3699–3705.

622 Bassett, H.R., Baumann, S., Campbell, G.S., Wiggins, S.M., Hildebrand, J.A., 2009. Dall's porpoise (
623 Phocoenoides dalli) echolocation click spectral structure. J. Acoust. Soc. Am. 125, 2677–2677.

624 Beedholm, K., Møhl, B., 2006. Directionality of sperm whale sonar clicks and its relation to piston radiation
625 theory. J. Acoust. Soc. Am. 119, EL14.

626 Borchers, D.L., Stevenson, B.C., Kidney, D., Thomas, L., Marques, T.A., 2015. A Unifying Model for Capture–
627 Recapture and Distance Sampling Surveys of Wildlife Populations. J. Am. Stat. Assoc. 110, 195–204.

628 Branstetter, B.K., Moore, P.W., Finneran, J.J., Tormey, M.N., Aihara, H., 2012. Directional properties of
629 bottlenose dolphin (Tursiops truncatus) clicks, burst-pulse, and whistle sounds. J. Acoust. Soc. Am.
630 131, 1613–1621.

631 Carlén, I., Thomas, L., Carlström, J., Amundin, M., Teilmann, J., Tregenza, N., Tougaard, J., Koblitz, J.C.,
632 Sveegaard, S., Wennerberg, D., Loisa, O., Dähne, M., Brundiers, K., Kosecka, M., Kyhn, L.A., Ljungqvist,
633 C.T., Pawliczka, I., Koza, R., Arciszewski, B., Galatius, A., Jabbusch, M., Laaksonlaita, J., Niemi, J.,
634 Lyytinen, S., Gallus, A., Benke, H., Blankett, P., Skóra, K.E., Acevedo-Gutiérrez, A., 2018. Basin-scale
635 distribution of harbour porpoises in the Baltic Sea provides basis for effective conservation actions.
636 Biol. Conserv. 226, 42–53.

637 Clausen, K.T., Wahlberg, M., Beedholm, K., Deruiter, S., Madsen, P.T., 2011. Click communication in harbour
638 porpoises Phocoena phocoena. Bioacoustics 20, 1–28.

639 Cosentino, M., Guarato, F., Tougaard, J., Nairn, D., Jackson, J.C., Windmill, J.F.C., 2019. Porpoise click
640 classifier (PorCC): A high-accuracy classifier to study harbour porpoises (Phocoena phocoena) in the
641 wild. J. Acoust. Soc. Am. 145, 3427–3434.

642 Cranford, T.W., 2000. In Search of Impulse Sound Sources in Odontocetes. pp. 109–155.

643 Cranford, T.W., Amundin, M., Norris, K.S., 1996. Functional morphology and homology in the odontocete
644 nasal complex: Implications for sound generation. J. Morphol. 228, 223–285.

645 Deruiter, S.L., Bahr, A., Blanchet, M.-A., Hansen, S.F., Kristensen, J.H., Madsen, P.T., Tyack, P.L., Wahlberg,
646 M., 2009. Acoustic behaviour of echolocating porpoises during prey capture. J. Exp. Biol. 212, 3100–
647 3107.

648 Finneran, J.J., Branstetter, B.K., Houser, D.S., Moore, P.W., Mulsow, J., Martin, C., Perisho, S., 2014. High-
649 resolution measurement of a bottlenose dolphin's (Tursiops truncatus) biosonar transmission beam
650 pattern in the horizontal plane. J. Acoust. Soc. Am. 136, 2025–2038.

651 Frasier, K.E., Wiggins, S.M., Harris, D., Marques, T.A., Thomas, L., Hildebrand, J.A., 2016. Delphinid
652 echolocation click detection probability on near-seafloor sensors. J. Acoust. Soc. Am. 140, 1918–1930.

653 Gillespie, D., Chappell, O., 2002. An Automatic System for Detecting and Classifying the Vocalisations of
654 Harbour Porpoises. Bioacoustics 13, 37–61.

655 Gillespie, D., Gordon, J., Mchugh, R., Mclaren, D., Mellinger, D., Redmond, P., Thode, A., Trinder, P., Deng,
656 X.Y., 2008. PAMGUARD: Semiautomated, open source software for real-time acoustic detection and
657 localisation of cetaceans. Proc. Inst. Acoust. 30, 2547.

658 Götz, T., Antunes, R., Heinrich, S., 2010. Echolocation clicks of free-ranging Chilean dolphins
659 (Cephalorhynchus eutropia). J. Acoust. Soc. Am. 128, 563–566.

660 Hansen, M., Wahlberg, M., Madsen, P.T., 2008. Low-frequency components in harbor porpoise (Phocoena
661 phocoena) clicks: communication signal, by-products, or artifacts? J. Acoust. Soc. Am. 124, 4059–
662 4068.

663 Jensen, F.H., Johnson, M., Ladegaard, M., Wisniewska, D.M., Madsen, P.T., 2018. Narrow Acoustic Field of
664 View Drives Frequency Scaling in Toothed Whale Biosonar. Curr. Biol. 28, 3878-3885.e3.

665 Jensen, F.H., Wahlberg, M., Beedholm, K., Johnson, M., de Soto, N.A., Madsen, P.T., 2015. Single-click beam
666 patterns suggest dynamic changes to the field of view of echolocating Atlantic spotted dolphins
667 (Stenella frontalis) in the wild. J. Exp. Biol. 218, 1314–1324.

668 Johnson, M., Madsen, P.T., Zimmer, W.M.X., de Soto, N.A., Tyack, P.L., 2006. Foraging Blainville's beaked
669 whales (Mesoplodon densirostris) produce distinct click types matched to different phases of
670 echolocation. J. Exp. Biol. 209, 5038–5050.

671 Johnson, M., Madsen, P.T., Zimmer, W.M.X.X., Aguilar de Soto, N., Tyack, P.L., 2004. Beaked whales
672 echolocate on prey. Proc. R. Soc. London. Ser. B Biol. Sci. 271, S383–S386.

673 Johnson, M.P., Tyack, P.L., 2003. A digital acoustic recording tag for measuring the response of wild marine
674 mammals to sound. IEEE J. Ocean. Eng. 28, 3–12.

675 Koblitz, J.C., Stilz, P., Rasmussen, M.H., Laidre, K.L., 2016. Highly Directional Sonar Beam of Narwhals
676 (Monodon monoceros) Measured with a Vertical 16 Hydrophone Array. PLoS One 11, e0162069.

677 Koblitz, J.C., Wahlberg, M., Stilz, P., Madsen, P.T., Beedholm, K., Schnitzler, H.-U., 2012. Asymmetry and
678 dynamics of a narrow sonar beam in an echolocating harbor porpoise. J. Acoust. Soc. Am. 131, 2315.

679 Küsel, E.T., Mellinger, D.K., Thomas, L., Marques, T.A., Moretti, D., Ward, J., 2011. Cetacean population
680 density estimation from single fixed sensors using passive acoustics. J. Acoust. Soc. Am. 129, 3610–
681 3622.

682 Kyhn, L.A., Tougaard, J., Beedholm, K., Jensen, F.H., Ashe, E., Williams, R., Madsen, P.T., 2013. Clicking in a
683 Killer Whale Habitat: Narrow-Band, High-Frequency Biosonar Clicks of Harbour Porpoise (Phocoena
684 phocoena) and Dall's Porpoise (Phocoenoides dalli). PLoS One 8, e63763.

685 Kyhn, L.A., Tougaard, J., Jensen, F., Wahlberg, M., Stone, G., Yoshinaga, A., Beedholm, K., Madsen, P.T.,
686 2009. Feeding at a high pitch: source parameters of narrow band, high-frequency clicks from
687 echolocating off-shore hourglass dolphins and coastal Hector's dolphins. J. Acoust. Soc. Am. 125,

1783–1791.

Ladegaard, M., Jensen, F.H., Beedholm, K., Da Silva, V.M.F., Madsen, P.T., 2017. Amazon river dolphins (Inia geoffrensis) modify biosonar output level and directivity during prey interception in the wild. J. Exp. Biol. 220, 2654–2665.

Ladegaard, M., Jensen, F.H., de Freitas, M., Ferreira da Silva, V.M., Madsen, P.T., 2015. Amazon river dolphins (Inia geoffrensis) use a high-frequency short-range biosonar. J. Exp. Biol. 218, 3091–3101.

Ladegaard, M., Madsen, P.T., 2019. Context-dependent biosonar adjustments during active target approaches in echolocating harbour porpoises. J. Exp. Biol. 222, jeb206169.

Li, S., Wang, D., Wang, K., Akamatsu, T., Ma, Z., Han, J., 2007. Echolocation click sounds from wild inshore finless porpoise (Neophocaena phocaenoides sunameri) with comparisons to the sonar of riverine N. p. asiaeorientalis. J. Acoust. Soc. Am. 121, 3938.

Madsen, P.T., Carder, D.A., Bedholm, K., Ridgway, S.H., 2005. Porpoise Clicks From a Sperm Whale Nose—Convergent Evolution of 130 Khz Pulses in Toothed Whale Sonars? Bioacoustics. 15, 195-206.

Madsen, P. T., de Soto, N.A., Arranz, P., Johnson, M., 2013. Echolocation in Blainville's beaked whales (Mesoplodon densirostris). J. Comp. Physiol. A Neuroethol. Sensory, Neural, Behav. Physiol. 199, 451–469.

Madsen, P.T., Lammers, M., Wisniewska, D., Beedholm, K., 2013. Nasal sound production in echolocating delphinids (Tursiops truncatus and Pseudorca crassidens) is dynamic, but unilateral: clicking on the right side and whistling on the left side. J. Exp. Biol. 216, 4091–4102.

Madsen, P.T., Surlykke, A., 2013. Functional Convergence in Bat and Toothed Whale Biosonars. Physiology 28, 276–283.

Madsen, P.T., Wahlberg, M., 2007. Recording and quantification of ultrasonic echolocation clicks from free-

ranging toothed whales. Deep Sea Res. Part I Oceanogr. Res. Pap. 54, 1421–1444.

Madsen, P.T., Wisniewska, D., Beedholm, K., 2010. Single source sound production and dynamic beam formation in echolocating harbour porpoises (Phocoena phocoena). J. Exp. Biol. 213, 3105–3110.

Malinka, C.E., Atkins, J., Johnson, M.P., Tønnesen, P., Dunn, C.A., Claridge, D.E., Aguilar de Soto, N., Madsen, P.T., 2020. An autonomous hydrophone array to study the acoustic ecology of deep-water toothed whales. Deep Sea Res. Part I Oceanogr. Res. Pap. 103233.

Marques, T.A., Thomas, L., Martin, S.W., Mellinger, D.K., Ward, J.A., Moretti, D.J., Harris, D., Tyack, P.L., 2013. Estimating animal population density using passive acoustics. Biol. Rev. Camb. Philos. Soc. 88, 287–309.

Martin, M.J., Gridley, T., Elwen, S.H., Jensen, F.H., 2018. Heaviside's dolphins (Cephalorhynchus heavisidii) relax acoustic crypsis to increase communication range. Proc. R. Soc. B Biol. Sci. 285, 20181178.

Melcón, M.L., Failla, M., Iñíguez, M.A., Melcón, M.L., Failla, M., Iñíguez, M. a., 2012. Echolocation behavior of franciscana dolphins (Pontoporia blainvillei) in the wild. J. Acoust. Soc. Am. 131, EL448–EL453.

Møhl, B., Wahlberg, M., Madsen, P.T., Heerfordt, A., Lund, A., 2003. The monopulsed nature of sperm whale clicks. J. Acoust. Soc. Am. 114, 1143–1154.

Møhl, B., Wahlberg, M., Madsen, P.T., Miller, L. a, Surlykke, a, 2000. Sperm whale clicks: directionality and source level revisited. J. Acoust. Soc. Am. 107, 638–648.

Morisaka, T., Connor, R.C., 2007. Predation by killer whales (Orcinus orca) and the evolution of whistle loss and narrow-band high frequency clicks in odontocetes. J. Evol. Biol. 20, 1439–1458.

Nelder, J.A., Mead, R., 1965. A Simplex Method for Function Minimization. Comput. J. 7, 308–313.

Park, S.W., Linsen, L., Kreylos, O., Owens, J.D., Hamann, B., 2006. Discrete Sibson interpolation. IEEE Trans. Vis. Comput. Graph. 12, 243–253.

732 Press, W.H., Teukolsky, S.A., 1990. Savitzky-Golay Smoothing Filters. Comput. Phys. 4, 669.

733 Rodrigues, O., 1840. es lois géometriques qui regissent les déplacements d' un systéme solide dans l'
734 espace, et de la variation des coordonnées provenant de ces déplacement considérées indépendant
735 des causes qui peuvent les produire. J. Math. Pures Appl. 5, 380–440.

736 Schrøder, A.E.M., Beedholm, K., Madsen, P.T., 2017. Time-varying auditory gain control in response to
737 double-pulse stimuli in harbour porpoises is not mediated by a stapedial reflex. Biol. Open 6, 525–529.

738 Silber, G.K., 1991. Acoustic signals of the vaquita (Phocoena sinus). Aquat. Mamm. 17, 130-133.

739 Smith, A.B., Kloepper, L.N., Yang, W.-C., Huang, W.-H., Jen, I.-F., Rideout, B.P., Nachtigall, P.E., 2016.
740 Transmission beam characteristics of a Risso's dolphin (Grampus griseus). J. Acoust. Soc. Am. 139,
741 53–62.

742 Sørensen, P.M., Wisniewska, D.M., Jensen, F.H., Johnson, M., Teilmann, J., Madsen, P.T., 2018. Click
743 communication in wild harbour porpoises (Phocoena phocoena). Sci. Rep. 8, 9702.

744 Stevenson, B.C., 2016. Methods in spatially explicit capture-recapture. University of St Andrews.

745 Stevenson, B.C., Borchers, D.L., Altwegg, R., Swift, R.J., Gillespie, D.M., Measey, G.J., 2015. A general
746 framework for animal density estimation from acoustic detections across a fixed microphone array.
747 Methods Ecol. Evol. 6, 38–48.

748 Strother, G.K., Mogus, M., 1970. Acoustical Beam Patterns for Bats: Some Theoretical Considerations. J.
749 Acoust. Soc. Am. 48, 1430–1432.

750 Verfuß, U.K., Miller, L.A., Pilz, P.K.D., Schnitzler, H.U., 2009. Echolocation by two foraging harbour porpoises
751 (Phocoena phocoena). J. Exp. Biol. 212, 823–834.

752 Villadsgaard, A., Wahlberg, M., Tougaard, J., 2007. Echolocation signals of wild harbour porpoises,
753 Phocoena phocoena. J. Exp. Biol. 210, 56–64.

754 Wisniewska, D.M., Johnson, M., Beedholm, K., Wahlberg, M., Madsen, P.T., 2012. Acoustic gaze
755 adjustments during active target selection in echolocating porpoises. J. Exp. Biol. 215, 4358–73.

756 Wisniewska, D.M., Ratcliffe, J.M., Beedholm, K., Christensen, C.B., Johnson, M., Koblitz, J.C., Wahlberg, M.,
757 Madsen, P.T., 2015. Range-dependent flexibility in the acoustic field of view of echolocating porpoises
758 (Phocoena phocoena). Elife 4, 1–16.

759 Yovel, Y., Falk, B., Moss, C.F., Ulanovsky, N., 2010. Optimal Localization by Pointing Off Axis. Science (80-.).
760 327, 701–704.

761 Zimmer, W.M.X., Harwood, J., Tyack, P.L., Johnson, M.P., Madsen, P.T., 2008. Passive acoustic detection of
762 deep-diving beaked whales. J. Acoust. Soc. Am. 124, 2823–2832.

763 Zimmer, W.M.X., Tyack, P.L., Johnson, M.P., Madsen, P.T., 2005. Three-dimensional beam pattern of
764 regular sperm whale clicks confirms bent-horn hypothesis. J. Acoust. Soc. Am. 117, 1473–1485.

765